RSC Advances

ROYAL SOCIETY OF CHEMISTRY

www.rsc.org/advances

Journal Name

ARTICLE TYPE

Fostering the properties of $Zr_{0.8}Sn_{0.2}TiO_4$ (ZST) ceramics via freeze granulation without sintering additives

S. M. Olhero[a],*, Ajay Kaushal[a],** and J. M. F. Ferreira[a]

The present paper reports on the overall benefits of freeze granulation for enhancing the properties of zirconium tin titanate, $Zr_{0.8}Sn_{0.2}TiO_4$ (ZST) ceramics in the total absence of sintering additives. The ZST powder was synthesized by solid state reaction and attrition milled in ethanol for 10 h. This starting non-granulated powder (NG–ZST), without and with 1 wt.% ZnO as sintering additive, was used to 10 consolidate green bodies by dry pressing. The pure ZST powder was also dispersed in aqueous media to obtain stable suspensions with high solid loadings. Free flowing spherical homogeneous granules were prepared by freeze granulation and used to consolidated ZST green bodies by dry pressing (FG–ZST). The effects of processing variables and of sintering temperature (1300–1450 ℃) on densification and on the structural, mechanical and electrical properties of ZST ceramics were systematically investigated. Our 15 study clearly reveals the superior properties of FG–ZST ceramics, which derive from an enhanced sintering behaviour associated to the absence of sintering additives.

A Introduction

The synthesis and structural characterization of zirconium titanate ($ZrTiO_4$) based materials for applications as resonators 20 components in microwave devices have recently attracted considerable and growing interest. [1] $ZrTiO_4$ ceramic material exhibits the α-PbO orthorhombic structure which transforms into the rutile structure of $TiO_2(SnO_2)$ at a certain Sn content. When Zr ions are substituted with Sn ions, a temperature stable 25 $(Zr,Sn)TiO_4$ microwave resonator is obtained by interfering with ordering of metal ions that results in improved dielectric properties. There is a phase boundary at x = 0.3 in $Zr_{1-x}Sn_xTiO_4$; at x < 0.3, a single phase $(Zr,Sn)TiO_4$, exists; but for x > 0.3, secondary phases of rutile $(Ti,Sn)O_2$ coexist with $(Zr,Sn)TiO_4$. [2,3] 30 Therefore, the solid solutions of zirconium tin titanate ($Zr_{1-x}Sn_xTiO_4$; $0 < x \leq 0.2$) have been regarded as potential materials for use in dielectric resonators or filters working at microwave frequency owing to their high quality factor (Q > 3000), high dielectric constant (ε_r > 25), and low temperature coefficient of 35 resonant frequency (TCF < ± 10 ppm ℃$^{-1}$). [4-10] The ZST ceramics are traditionally consolidated from spray-dried powders. Unfortunately, this granulation method is prone to the formation of cavities, strong interparticle bonds and migration of additives and/or smaller particles to the granule surface. Such 40 heterogeneities exacerbate the difficulties to fully densify $Zr_{1-x}Sn_xTiO_4$ ceramics without sintering aid additives. Some common sintering aids used for $Zr_{1-x}Sn_xTiO_4$ ceramics are added as a combination of two or more oxides from the group consisting of ZnO, CuO, La_2O_3, NiO, Fe_2O_3, B_2O_3, Bi_2O_3, and V_2O_5. [11-14]

45 However, sintering aids affect the ceramics in many ways by changing density, microstructure, defect structure, and possibly crystal structure. These changes, brought about by the sintering aids, affect the resulting dielectric properties. Many earlier investigations on $Zr_{1-x}Sn_xTiO_4$ compositions and other microwave 50 dielectrics showed that the selection of proper additives and their optimum quantity are effective in enhancing the dielectric properties. A higher relative density results in a higher dielectric constant. [15,16] Therefore, improving the sintering ability and the various functional properties of zirconium tin titanate ceramics 55 without using sintering aids has been a challenging task. Accomplishing this task demands an upgrade in the powder processing approach, in order to improve particle packing ability and getting high dense and homogeneous green compacts upon consolidation. Such potential gains derived from processing could 60 be a way to exclude the sintering additives from $Zr_{1-x}Sn_xTiO_4$ compositions. Our recent findings, [15,17,18] stimulated us to achieve successful aqueous colloidal processing of $Zr_{1-x}Sn_xTiO_4$ composition and further preparing high quality spherical granules by freeze granulation (FG), resulting in ceramics with high green 65 dense compact on consolidation. FG can help ceramic manufacturers achieving powder formulations with superior homogeneity, pressing performance and dispersability. [19-21] During FG, droplets are rapidly frozen in liquid nitrogen before being recovered and subsequently freeze-dried. Freezing being a 70 fast process, diffusion dynamics are insufficient to induce any binder migration, thereby better preserving the granule homogeneity. [22,23] Contrary to spray drying, the freeze dried granules do not shrink during freeze drying, maintaining their spherical shapes and consequently allowing high granule

deformability. Recognizing the advantages of FG, Stuer *et al.* [20] adopted FG powders as an industrially viable alternative to loose powder for sintering transparent polycrystalline alumina. Hence, the FG method provides granules with high degree of homogeneity that easily can be broken down in a subsequent processing step such as pressing or re-dispersing in a liquid. The composition $Zr_{0.8}Sn_{0.2}TiO_4$ (ZST) was chosen for the present investigation as it is phase pure and stable against thermal decomposition. [24] The ZST powder with this composition was successfully dispersed in water and the suspension was sprayed against liquid nitrogen to obtain homogeneous granules. The benefits of FG for the consolidation/sintering steps were highlighted by comparing the green and sintered density values of ZST ceramics prepared by dry pressing from FG powder, and non-granulated powders (NG) without and with 1 wt.% ZnO as sintering additive. The effects of sintering temperature (T_{sint}) that was varied within the range from 1300 to 1450 °C on the various structural, mechanical and dielectric properties of the as obtained ZST ceramics were investigated. The search was for processing conditions that could lead to low-loss dielectric ZST materials within the microwave frequency range.

B Experimental

B.1 Powder synthesis

The zirconium tin titanate powder (ZST) ($Zr_{0.8}Sn_{0.2}TiO_4$) was synthesized through the conventional solid state reaction process from high purity ZrO_2 (Zirconium oxide, Sigma-Aldrich, Steinheim, Germany), SnO_2 (tin IV oxide, Sigma-Aldrich, Steinheim, Germany) and TiO_2 (Titanium IV Oxide, Riedel-de Haen, Sielze, Germany). The starting raw materials were mixed according to the required stoichiometric proportions and dry ball-milled for 2 h to guarantee complete homogenisation. The precursor mixture was firstly calcined at 1100 °C for 2 h, dry ball-milled for 2 h, and then submitted to a second heat treatment for 2 h at 1350 °C. In order to reduce particle size of the calcined powder, attrition milling at 700 rpm speed in ethanol was conducted for 10 h. The efficacy of the deagglomeration progress was monitored by particle size analysis using a light scattering technique (Beckman Coulter LS 230, CA USA; Fraunhofer optical model). For this, approximately 0.1 g of dry milled powder was dispersed into 50 ml of distilled water followed by 20 minute ultrasonic treatment to separate the powder particles. The resultant diluted suspension was analyzed for particle size distribution. Three measurements per sample were performed to confirm the reproducibility of the distribution curves. The resultant ZST slurry was dried at 110 °C and characterised by X-ray diffraction (Rigaku, Tokyo, Japan), specific surface area (BET, Gemini, Micromeritics, USA) and helium pycnometry (Multypicnometer, Quantachrome Instruments, USA), and used for the further studies in the pure non-granulated (NG–ZST) and freeze granulated (FG–ZST) forms, and with the addition of 1 wt.% ZnO as sintering additive as detailed below.

B.2 Investigating the effects of freeze granulation and ZnO-doping

Successful freeze granulation requires a suitable balance between low viscosity and high concentrated suspensions. Therefore, the dispersion ability of the ZST powder in aqueous media was firstly investigated to establish the optimal processing conditions. The potential at the solid/liquid interface was assessed by zeta-potential measurements (Delsa 440 Sx, Coulter, Buckinghamshire, UK) in the absence and in the presence of dispersant (Dispex A40). The powders were suspended into a 1 mM KCl solution as background electrolyte to assure a constant ionic strength. Each suspension was divided in two equal parts for increasing and decreasing pH runs, and the pH values were adjusted by using 0.1 M solutions of either KOH or HCl, respectively. The efficacy of Dispex A40 in dispersing the ZST powder was further confirmed by the easiness how aqueous slurries containing 40, 45 and 50 vol.% could be prepared with 0.5 wt.% added dispersant. The suspensions were deagglomerated for 24 h in polypropylene bottles using zirconia balls (the charge to balls ratio was 1:3). The viscosity of slurries was measured using a rotational Rheometer (Bohlin C−VOR Instruments, Worcestershire, UK) equipped with a cone and plate (4°, 40 mm, and gap of 150 μm) measuring configuration. The flow measurements were conducted between 0.1 and 500 s^{-1}. A binder emulsion (Duramax D1000, Rohm and Haas, Lauterbourg, France) was added (3 wt.% relative to the dry powder) to the ZST suspension containing 45 vol.%. This aqueous suspension was sprayed into liquid nitrogen (−196 °C) to obtain granules by freeze granulation (Power Pro freeze granulator LS−2, Gothenburg, Sweden). LS-2 freeze granulator consists of a slip container with a stirrer, a pump for the slip, a spray nozzle, a regulator for compressed air and an insulated chamber for liquid nitrogen to spray and collect freeze granules. Prior to granulation process, the ZST suspension was filtered using a 120 μm sieve to safely avoid any agglomeration that may obstruct the flow through the 1.20 mm diameter granulation nozzle. For successful micro sized ZST granulation, the suspension was sprayed at a pumping speed of 30 rpm with ~ 0.8 bar air pressure. A drying step at −49 °C under a pressure of 0.133 Pa (1×10^{-3} torr) in a freeze-drying system (Labconco, LYPH Lock 4.5, Kansas City, MO) was then conducted for 72 h. The freeze dried (FG–ZST) granules were uniaxial pressed into disc-shaped pellets (20 mm diameter, 3−5 mm thickness) and bars (50 mm × 5 mm × 5 mm) at a uniaxial pressure of 60 MPa, followed by isostatic pressing at 200 MPa.

Dry pressing was similarly adopted to consolidate green bodies from the starting powder, either pure (NG–ZST) or doped with ZnO as sintering additive. In this last case, the starting NG–ZST powder was mixed in ethanol with 1 wt.% ZnO (NG–ZST–ZnO) followed by drying. The same type and amount of binder (Duramax D1000, 3 wt.% relative to the dry mass) was added to the dried NG–ZST and NG–ZST–ZnO powders by spraying and mixing in a mortar. Binder burnout of all samples was performed at a heating rate of 1 °C min^{-1} up to 600 °C, with holding time of 1 h at this temperature. Sintering was performed at different temperatures (1300, 1350, 1400 and 1450 °C) at a heating rate of 5 °C min^{-1}, holding for 4 h at the set temperature, followed by natural cooling. Dilatometry measurements were performed on
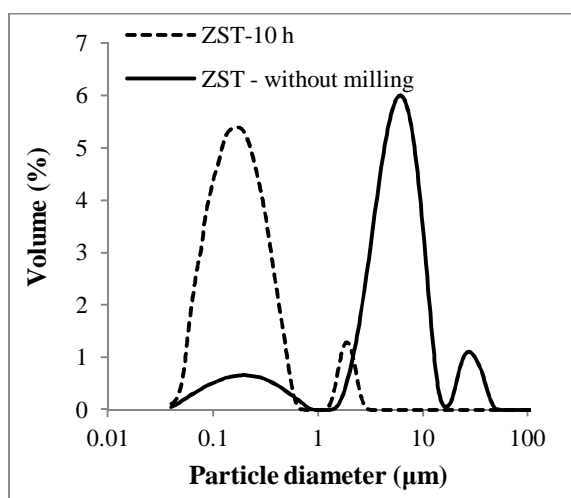
Fig 1. Particle size distribution of the ZST powder as synthesized (without milling) and after 10 h of attrition milling

bar shaped (50 mm × 5 mm × 5 mm) green samples of NG–ZST, FG–ZST, and NG–ZST FG using a Dil 801L dilatometer (BAHR Thermoanalyse, GmbH Adidi 4.0, Germany). The complete dilatometric shrinkage data were measured from room
5 temperature (RT) to 1400 ℃ at the heating rate of 10 ℃/minute in air atmosphere.

B.3 Characterization of ZST sintered samples

The crystallinity of the ZST synthesised powder and the sintered samples at different temperatures (1300–1450℃) were studied
10 using a Rigaku X-ray diffractometer of CuK_α (1.54 Å) radiations in θ–2θ geometry. Bulk density (ρ_{bulk}) of sintered ZST ceramics was measured in ethylene glycol according to the Archimedes principle (ASTM C372, ASTM International, West Conshohocken, PA) using a Mettler balance (AG 245, Mettler
15 Toledo, Zurich, Switzerland). Three density measurements were performed for each kind of ceramic sample and the results are expressed as the average. The maximum experimental error was systematically < ± 0.01. Surface fracture microstructures of sintered ceramics were obtained by scanning electron microscopy
20 (SEM, JSM-5410, JEOL, Tokyo, Japan) with an energy-dispersive scanning attachment (Sigma 3.42 Quaser, Kevex, Stanford, Valencia, CA).

Vickers micro hardness measurements were performed on sintered and polished ZST samples using Struers Duramin testing
25 equipment (Struers, Denmark). Three point bending tests were conducted in a Shimadzu Autograph AG-X-1kN Universal Testing Machine (Kyoto, Japan). The cavity method was used for the measurement of dielectric constant and quality factor. In this method, we measure the shift in the resonant frequency of the
30 cavity, Δf, caused by the sample, and is related to the real part of the complex permittivity, ε′, while the change in the inverse of the quality factor of the cavity, Δ(1/Q), gives the imaginary part, ε″. The measurements were made using a HP 8753D and a HP8361 Network Analyzers coupled to 1.0 GHz and 6.0 GHz
35 cavity resonators

C Results and discussion

C.1 ZST powders and suspensions

Figure 1 shows particle size distribution (PSD) of sintered ZST powders before (dry ball milled for 1 h) and after wet attrition
40 milling (AM) for 10 h in ethanol. The powder dry milled for 1 h has an average particle size of ~9 μm and exhibits a trimodal distribution with small fine and coarse populations centred at ~0.2 μm and ~27 μm, respectively, and a main intermediate population centred at ~6 μm. Both the intermediate and
45 (especially) the coarser populations reveal the presence of particle agglomerates. Attrition milling destroyed completely the third population of agglomerates; reduced drastically the second one and shifting the remaining part to smaller sizes, while significantly increasing the finest population of particles. The
50 resulting AM powder with an average particle size of ~0.4 μm exhibits a bimodal size distribution adequate to prepare high concentrated colloidal suspensions. A bimodal PSD enhances the packing ability of the system and decreases the viscosity of a suspension at a given solid loading, facilitating the flow through a
55 fine nozzle during freeze granulation. The resultant ZST powder after 10 h AM presented a BET specific surface area of 3.2 m² g⁻¹ and a theoretical density of 5.19 g cm⁻³.

In order to assess the effects of dispersant (Dispex A-40) on the electrostatic repulsion between the ZST particles, zeta
60 potential measurements were performed in the absence and in the presence of dispersant. The curves displayed in Figure 2 reveal an isoelectric point (IEP) at pH ≈ 3 for the naked ZST particles and a dislocation of the entire electrophoretic curve towards more negative zeta potential values lower slightly towards acidic
65 region. This resulted in a shift of the IEP to pH ≈ 2. It is well known that for low values of zeta potential, intermolecular attractive forces between particles tend to exceed the electrostatic repulsive ones, resulting in a flocculated system. An opposite scenario is required for colloidal particles to form stable
70 suspensions. The zeta potential values measured at the natural pH of the suspensions in presence of dispersant (pH ≈ 9) are high enough (−80 mV) to keep high repulsion between particles and consequently, for allowing the preparation of high concentrated suspensions of ZST powders in aqueous media. This is confirmed
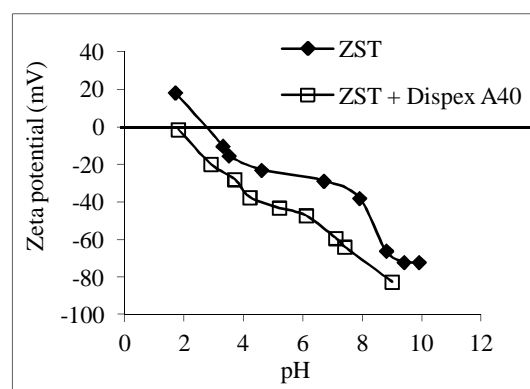

Fig 2. Zeta potential of the ZST powder in the absence and in the presence of dispersant.
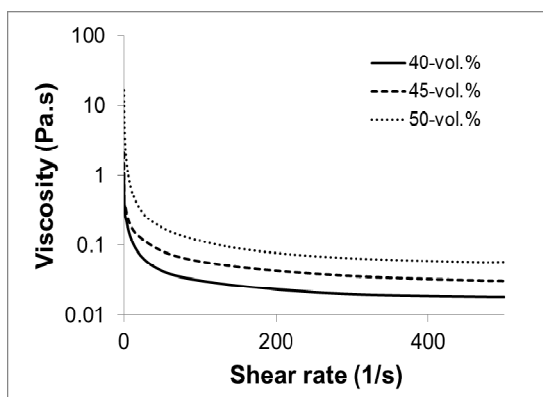
Fig 3. Flow curves of the ZST suspensions in aqueous media containing different solid loadings (40, 45 and 50 vol.%).
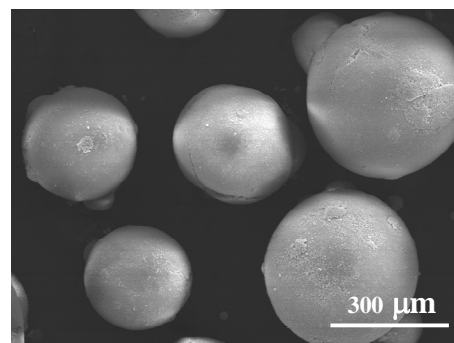

Fig 4. ZST granules (green state) obtained by freeze granulation from an aqueous suspension containing 45 vol.% solids.

by the rheological measurements performed on ZST suspensions with different solid loadings (Φ = 40, 45 and 50 vol.%) within the range from $\dot{\gamma}$ = 0.1 – 500 s^{-1}. The viscosity (η_s) *vs* shear rate ($\dot{\gamma}$) dependence curves presented in Figure 3 show that all suspensions displayed shear thinning behaviour within the entire $\dot{\gamma}$ range, a characteristic of well-dispersed and highly concentrated systems. The shear thinning flow behaviour reveals that particle aggregates in the suspensions are gradually broken down into smaller flow units by the applied forces, so that the resistance to flow is reduced leading to the lower viscosity as the shear rate increases. The particles become less and less interactive as the solid volume fraction decreases. The ZST suspension with 45 vol.% solid loading was selected to prepare granules by FG. Figure 4 shows SEM images of green ZST granules obtained by freeze-drying. Spherical granules with diameters within the range of few hundreds of micrometres were obtained. These morphological/size features confer them free flow behaviour and low friction with die walls upon dry pressing, which are essential features for obtaining homogeneous and highly dense ZST compacts.

C.2 Structural properties of sintered ZST ceramics

Figure 5 shows the XRD patterns of the pure ZST ceramics sintered at different T_{sint} of 1300, 1350, 1400 and 1450 °C. All the diffraction peaks of the ZST ceramics correspond to orthorhombic type phase structure in agreement with the respective Joint Committee on Powder Diffraction Standards (JCPDS) card No. 01-081-2214, and are in good consistency with results reported elsewhere. [25] The intensity of dominant peak (observed at ~31 °) was found to increase with increase in T_{sint}. This apparent enhancement of crystallinity of ZST phase is probably due to favoured crystal growth kinetics with rising temperature.

Table 1 reports on the physical/mechanical properties [relative density (ρ_r), micro-hardness and flexural resistance] of the investigated ZST ceramics sintered at different temperatures. Irrespective of the specific processing parameters used, a general increasing trend of ρ_r with increase in T_{sint} is observed. Interestingly, significantly higher ρ_r values were measured for the samples consolidated from the freeze granulated (FG–ZST)

powder in comparison to those derived from the non-granulated (NG–ZST) one. In this last case, ρ_r changed from 84% (1300 °C) to 93% (1450 °C) (based on the theoretical density of ZST = 5.19 g cm^{-3}). This last value is even 2.4% lower than that achieved for FG–ZST compacts upon sintering at the lowest sintering temperature tested (1300 °C). The observed differences suggest that the diffusion paths have been shortened in the samples derived from the FG powder due to their higher degree of homogeneity. Generally, micron-sized granules obtained by freeze granulation exhibit a number of favourable features in comparison to loose powders or granules obtained by spray drying as follows: (i) lower green density in comparison to granules obtained by spray drying; (ii) are homogeneous (no binder segregation occurs); (iii) free-flowing behaviour that enables their spatial rearrangements; and (iv) are easily smashed under the applied pressure. These features favour the elimination of the intergranular pores. The binder in FG granules acts as
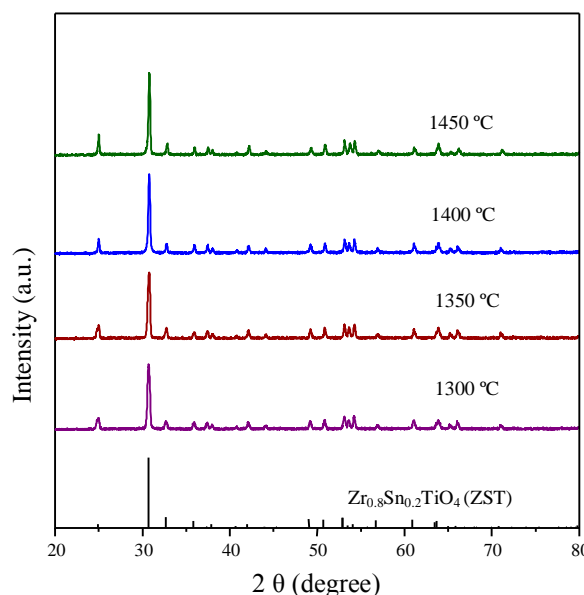

Fig 5. XRD patterns of pure $Zr_{0.8}Sn_{0.2}TiO_4$ (ZST) ceramics sintered at different temperatures (1300, 1350, 1400, 1450 °C).

Table 1 Relative density, microhardness and flexural resistance of ZST samples consolidated by dry pressing from ZST powders non–granulated (NG–ZST), freeze granulated (FG–ZST) and non–granulated with added 1 wt.% ZnO as sintering additive (NG–ZST–ZnO).

Samples	T_{sint} (ºC)	Relative density, ρ_r (% TD)	Microhardness (MPa)	Flexural resistance (MPa)
NG–ZST	1300	84.0 ± 1.6	----	54.0 ± 11.7
	1350	87.6 ± 7.6	1226.3 ± 165.6	74.3 ± 14.1
	1400	89.4 ± 3.2	4030.5 ± 719.4	87.6 ± 20.8
	1450	93.0 ± 0.7	6610.2 ± 500.2	119.2 ± 43.3
FG–ZST	1300	96.4 ± 2.4	3602.2 ± 249.7	104.0 ± 16.3
	1350	96.9± 1.2	6248.4 ± 481.2	141.3 ± 8.1
	1400	98.7 ± 0.7	9527.0 ± 441.3	179.7 ± 45.8
	1450	97.2 ± 0.4	9135.1 ± 433.3	157.2 ± 17.4
NG–ZST–ZnO	1300	96.9 ± 0.5	4189.7 ± 549.2	121.2 ± 36.6
	1350	97.4 ± 1.8	6893.2 ± 379. 8	154.4 ± 27.0
	1400	98.9 ± 0.9	9679.1 ± 563.1	181.8 ± 13.7
	1450	97.5 ± 0.7	9372.3 ± 491.5	167.5 ± 23.9

lubricant, assisting primary particles sliding and rearranging to increase the packing efficiency and compact density. An increase in packing efficiency and compact density will enhance the densification ability upon sintering while implying a decrease of total shrinkage. [15, 18] This is confirmed by the data plotted in Figure 6 that compares the dilatometry curves of all kinds of powder compacts (FG–ZST, NG–ZST and NG–ZST–ZnO) monitored within the temperature from room temperature (RT) to 1400 ºC. The FG–ZST curve exhibits a negative inclination along the lower temperature range, probably due to the homogeneous distribution of binder among the particles and its burnout enables the particles to gradually approach each other. The positive inclination observed for NG–ZST and NG–ZST–ZnO curves reveals that thermal expansion along this lower temperature range predominates over any shrinkage. Figure 6 reveals that the onset of shrinkage due to sintering occurs earlier (~950 ºC) and progresses at a much faster rate for the NG–ZST–ZnO sample, which achieved a minimum in the curve at ~1260 ºC followed by
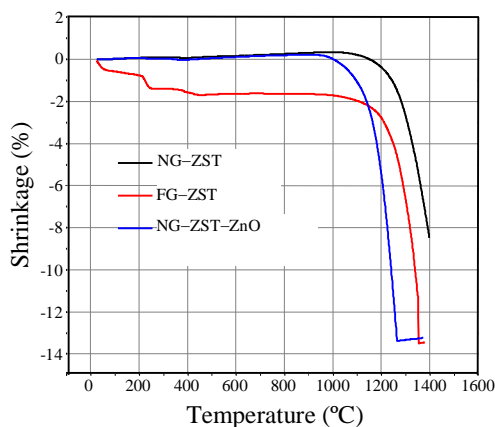
a slop reversion due to the predominance of dilatation over shrinkage. This effect justifies the use of ZnO as sintering additive. [12, 13] The onset of shrinkage due to sintering for the NG–ZST occurs roughly at ~1050 ºC and its densification process was still far from completion at the maximum tested temperature of 1400 ºC. Oppositely, a downshift of ~50 ºC in the onset of shrinkage and much faster densification kinetics are observed in the case of FG–ZST. These features clearly evidence the benefits of freeze granulation, being a viable route in getting high density pure ZST ceramics and avoiding external doping that might compromise the functional properties. The ρ_r values of FG–ZST and NG–ZST–ZnO ceramics sintered at 1400 ºC are close to ~99 %, and their mechanical properties (microhardness and flexural resistance) are also comparable (Table 1). Slightly decreasing trends are observed for ρ_r and mechanical properties of the FG–ZST and NG–ZST–ZnO samples with further increasing T_{sint} to 1450 ºC. These are attributed to an over firing effect as suggested by the increasing size of intergranular pore as seen in SEM micrographs of fracture surfaces shown in Figure 7. Figure 7 (a-f) shows SEM images of polished surfaces of NG-ZST, FG-ZST and NG-ZST-ZnO ceramics sintered at high T_{sint} of 1400 and 1450 ºC, revealing different microstructural features. The selection of these two high T_{sint} to investigate the microstructural features was based on the dilatometric curves, which suggested that maximum densification has been achieved for FG-ZST and NG-ZST-ZnO, contrasting with the NG-ZST ceramics. These SEM images reveal different morphological features that reflect different sintering ability between FG-ZST and NG-ZST ceramics, which derive solely from the powders being or not freeze granulated and how this processing step affects consolidation. In case of NG-ZST ceramics, the porosity fraction was found to decrease with increase in T_{sint} from 1400 ºC to 1450 ºC (Fig. 7a-b), in good agreement with density data reported in Table 1 that showed a steady increase from 84 to 93% with sintering temperature increasing from 1300–1450 ºC. This contrasts with the observations made for FG-ZST and NG-ZST-ZnO ceramics sintered at 1400 ºC and 1450 ºC (Fig. 7c-f) that
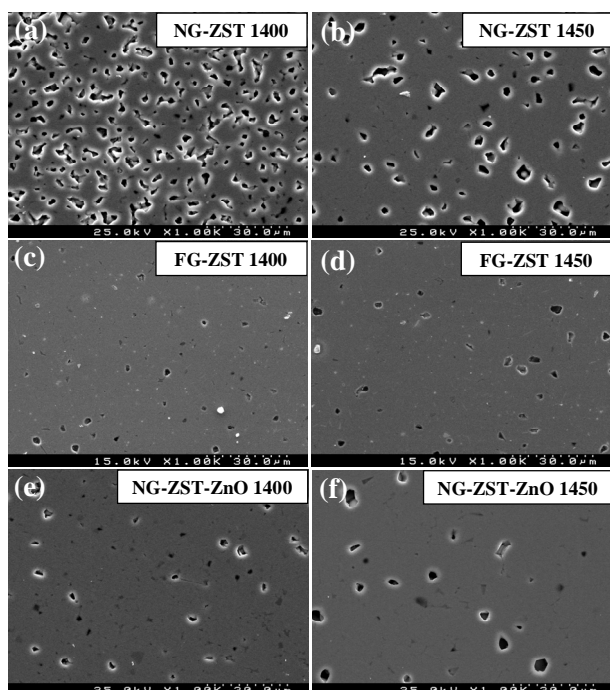

Fig 6. Dilatometry analysis of green bodies consolidated from powders NG–ZST, FG–ZST, and NG–ZST with added 1 wt.% ZnO as sintering additive (NG–ZST–ZnO) performed within the temperature range from RT to 1400 ºC.

Fig 7. SEM images of polished surfaces of ZST ceramics derived from NG–ZST, FG–ZST and NG–ZST–ZnO powders revealing the effects of processing variables and sintering temperature (1400 and 1450 ºC) on the microstructural features.

show larger pores derived from pore coalescence. These structural changes suggest that an over firing effect has occurred in the FG and ZnO added ZST ceramics sintered at 1450 ºC, in good agreement with density data reported in Table 1. These
5 results confirm that all the thermal events occur at lower temperatures for ceramics consolidated from FG powder due to its enhanced homogeneity in comparison to ceramics derived from NG powders.

The larger crystallite size FG-ZST ceramics in comparison to
10 that of NG-ZST ones can easily be explained in terms of diffusion kinetics. The compacts derived from uniform FG-ZST powders enable obtaining a homogeneous distribution of fine pores and higher green densities in comparison to NG-ZST ones. These conditions constitute the main driving force for diffusion
15 processes upon sintering that lead to faster densification and grain growth in the case of FG-ZST samples. Upon sintering, most of the very small pores tend to disappear and the sintered density
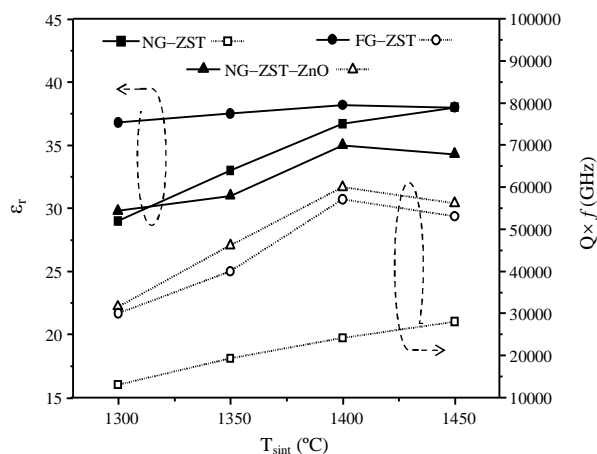

Fig 8. Dielectric constant (ε_r) (solid symbol and lines) and Q $\times$ f (open symbol and lines) measured at 6 GHz (microwave frequency) for ZST ceramics derived from NG–ZST, FG–ZST and NG–ZST–ZnO powders and sintered at different temperatures (1300, 1350, 1400 and 1450 ºC).

achieves a maximum value at a given temperature. Beyond this temperature, density is likely to decrease due to pore coalescence,
20 or the eventual formation of gases due to volatilisation of some components, phenomena known as over firing effect. This seems to have occurred in the FG-ZST and ZnO added ZST ceramics sintered at 1450 ºC.

**C.3 Microwave dielectric properties (Q factor) of ZST
25 ceramics**

Figure 8 shows the room temperature dielectric constant (ε_r) and quality factor (Q) values measured at 6 GHz (microwave frequency) for the NG–ZST, FG–ZST and NG–ZST–ZnO ceramics sintered at different T_{sint} of 1300, 1350, 1400 and 1450
30 ºC. The gathered data are also reported in Table 2. The ε_r values of the all prepared ZST ceramics were found to vary in the range from 25 to 38.2, with the highest one being observed for FG–ZST sintered at 1400 ºC. The NG–ZST–ZnO ceramics exhibit a maximum $\varepsilon_r = 35$ when sintered at 1400 ºC, being even lower that
35 that measured for NG–ZST ceramics. Except for the NG–ZST ceramics sintered at the lowest temperature, it can be stated that pure ZST ceramics exhibit higher ε_r values in comparison to the NG–ZST–ZnO ones. This confirms the deleterious effect for the dielectric constant of doping the ZST with 1 wt.% ZnO. On the

Table 2 Dielectric constant and Q $\times$ f factor of the ZST ceramics sintered at different temperatures and consolidated by dry pressing from ZST powders non-granulated (NG–ZST), freeze granulated (FG–ZST) and non-granulated with added 1 wt% ZnO as sintering additive (NG–ZST–ZnO).

T_{sint} (ºC)	Dielectric constant (ε_r) (at 6 GHz)			Q x f (at 6 GHz) (GHz)		
	NG–ZST	FG–ZST	NG–ZST–ZnO	NG–ZST	FG–ZST	NG–ZST–ZnO
1300	29.0	36.8	29.8	13043	30000	31579
1350	33.0	37.5	31.0	19286	40000	46156
1400	36.7	38.2	35.0	24182	57143	60000
1450	38.0	38.0	34.3	28000	53078	56154

other hand, the loss, quality factor (Q) values are the highest for the NG–ZST–ZnO ceramics at all T_{sint} range in comparison to pure ZST ceramics. This can be attributed to the larger grain sizes observed in the SEM micrographs of Fig. 7 with fewer grain boundaries contributing to the loss. But the Q values measured for FG–ZST are relatively close to those of NG–ZST–ZnO ceramics at any T_{sint} tested. The Q values for pure ZST ceramics were found to improve with increasing ρ_r and grain size, being significantly higher for the samples consolidated from FG powder and shown in Fig. 8. The maximum Q $\times$ f value of FG–ZST ceramics sintered at 1400 ºC (57143 GHz) is considerably higher than the maximum of 28000 GHz measured for NG–ZST ceramics sintered at 1450 ºC. The comparison of Fig. 8 with data reported in Table 1 and Table 2 enables concluding ε_r and Q $\times$ f values scale well with ρ_r and show good consistency with the microstructural features.

Conclusions

Micron-sized granules of ZST powder via freeze granulation method were successfully fabricated via spraying a stable aqueous suspension into liquid nitrogen (freeze granulation), followed by freeze drying. It was demonstrated that FG brings a number of benefits, including a higher degree of homogeneity in the binder distribution; an enhanced packing ability of the powders, and a faster sintering kinetics. These features enable improving the final physical/mechanical and dielectric properties of the ceramics and achieving the maximum at lower sintering temperatures. Another further advantage of the FG approach is the possibility to avoid the addition of sintering additives that might degrade the required functional properties. A maximum Q $\times$ f value of 57143 GHz was measured for the FG–ZST ceramics sintered at 1400 ºC, which is about double of that found for NG–ZST ceramics (28000 GHz) when sintered at a higher temperature of 1450 ºC. All the relevant physical and electrical properties of ZST ceramics revealed good correlations with sintered density, which in turn were shown to be strongly dependent on the quality of the processing translated by the homogeneity of the green compacts.

Acknowledgments

Notes and references

a Department of Materials and Ceramic Engineering, CICECO, University of Aveiro, 3810-193, Aveiro-Portugal. Fax: +351–234–370204; Tel.: +351–234–370354;
* E-mail: susana.olhero@ua.pt ; ** E-mail: ajay.kaushal@ua.pt

1   A. Borrell, M. D. Salvador, V. G. Rocha, A. Fernández, A. Gómez, E. López-López, R. Moreno, *Composites: Part B,* 2014, **56**, 330.
2   W. Wersing, "High Frequency ceramic dielectric and their application for microwave components", Ch 4 pp 67 in Electronic ceramics edited by B.C.H. Steele, Elsevier Science Publishers LTD, Barking, UK, 1991.
3   S. Hirano, T. Hayashi, A. Hattori, *J. Am. Ceram. Soc.*, 1991, **74**, 1320.
4   C-H. Hsu, *Thin Solid Films*, 2009, **517**, 5061.
5   C-H. Hsu, C-Y. Chung, *J. Alloys Comp.*, 2010, **491**, 483.
6   S. Genovesi, F. Costa, B. Cioni, V. Miceli, G. Annino, G. Gallone, G. Levita, A. Lazzeri, A. Monorchio, and G. Manara, *Microw. Opt. Techn. Lett.*, 2009, **51 [11]**, 2753.
7   P. G. Babu, C. Kumar, K. Ravichandran, and P. Manohar, *Inter. J. Chem. Tech. Res.*, 2013,**5 [5]**, 2122.
8   J-M. Wu, W-Z. Lu, W. Lei, J-P. He, J. Wang, *Ceram. Int.*, 2011, **37**, 481.
9   K. H. Yoon and E.S.W. Kim, *Mater. Res. Bull.*, 1995, **30 [7]**, 813.
10 G. Huang, D. Zhou, J. Xu, X. Chen, D. Zhang, W. Lu, B. Li, *Mater. Sci. Eng. B*, 2003, **99**, 416.
11 S. Vahabzadeh, M.A. Golozar, F. Ashrafizadeh, *J. Alloys Comp.*, 2011, **509**, 1129.
12 C-L. Huang, C-S. Hsu, R-J. Lin, *Mater. Res. Bull.,* 2001, **36**, 1985.
13 V. L. Abrantes, *J. Maters Eng. Perform.*, 2012, **21 [8]**, 1777.
14 V. L. Abrantes, D. P. F. de Souza, *Mater. Sci. Eng. A*, 2005, **398**, 220.
15 A. Kaushal, S.M. Olhero, P. Antunes, A. Ramalho, J.M.F. Ferreira, *Mater. Res. Bull.*, 2014, **50**, 329.
16 R. Kudesia, A. E. McHale and R. L. Snyder, *J. Am. Ceram. Soc.*, 1994, **77[12]**, 3215.
17 A. Kaushal, S. M. Olhero., J. M. F. Ferreira, *J. Mater. Chem. C*, 2013, **1**, 4846.
18   A. Kaushal, S. M. Olhero, B. K. Singh, V. Saravanan and J. M. F. Ferreira, RSC Adv., **4**, 26993-27002, 2014.
19 B. Nyberg, E. Carlstrom and R Carlsson, "Freeze granulation of liquid phase sintered silicon carbide" pp 107-113 in Ceramic transaction, vol. 42, Silicon-Based Structural Ceramics, Edited by Brian W. Sheldon and Stephen C. Denforth, Americal Ceramic Society, Westerville, Ohio, 1994.
20 M. Stuer, Z. Zhao, P. Bowen, *J Europ Ceram Soc*, 2012, **32**, 2899.
21 J. Orlenius, O. Lyckfeldt, K.A. Kasvayee, P. Johander, *J. Power Sources*, 2012, **213**, 119.
22 O. Lyckfeldt, D. Käck, K. Rundgren, *Ceram. Eng. Sci. Proc.*, 2003, **24 [4]**, 331.
23 O. Lyckfeldt, K. Rundgren, M. Sjöstedt, *Key. Eng. Mat.,* 2004, **264-268** [Part 1], 281.
24 Y. H. Park, J. M. Ryu, M. Y. Shin, K. H. Ko, D. W. Kim and K-S Hong, *J. Am. Ceram. Soc.*, 2001, **84**, 2542.
25 R. Kudesia, R.L. Snyder, R.A. Condrate, A.E. McHale, *J. Phys. Chem. Solids.*, 1993, **54**, 671.

RSC Advances Accepted Manuscript